



Carracedo, A., Rodes, A. , Smellie, J.L. and Stuart, F.M. (2019) Episodic erosion in West Antarctica inferred from cosmogenic ^3He and ^{10}Be in olivine from Mount Hampton. *Geomorphology*, 327, pp. 438-445. (doi:[10.1016/j.geomorph.2018.11.019](https://doi.org/10.1016/j.geomorph.2018.11.019))

There may be differences between this version and the published version. You are advised to consult the publisher's version if you wish to cite from it.

<http://eprints.gla.ac.uk/173848/>

Deposited on: 21 November 2018

Enlighten – Research publications by members of the University of
Glasgow

<http://eprints.gla.ac.uk>

1 **Episodic erosion in West Antarctica inferred from cosmogenic ^3He**
2 **and ^{10}Be in olivine from Mount Hampton**

3 A. Carracedo^{1,*}, Á. Rodés¹, J. L. Smellie² and F.M. Stuart¹

4 ¹ Isotope Geosciences Unit, Scottish Universities Environmental Research Centre, Rankine
5 Avenue, East Kilbride G75 0QF, UK

6 ² Department of Geology, University of Leicester, UK

7

8 *Corresponding author: anacp79@hotmail.com

9

10 **Abstract**

11 The polar climate of Antarctica results in the lowest erosion rates on Earth. The low
12 long-term erosion history of high elevation mountain tops that are exposed above the
13 ice preserve a record of climate change that can be accessed using cosmogenic nuclides.
14 However, unravelling the complexity of the long-term denudation histories of Antarctic
15 summits is frequently hampered by intermittent ice cover. The aim of this work is to
16 identify denudation rate changes in a surface that has been continuously exposed since
17 the middle Miocene. We have measured stable (^3He) and radioactive (^{10}Be) cosmogenic
18 nuclides in olivine from lherzolite xenoliths from the summit of the Mount Hampton
19 shield volcano within the West Antarctic Ice Sheet. The peak (3200 m) has never been
20 covered by the current ice sheet and local ice caps, consequently the data record the
21 subaerial erosion history of a mountain top within the Antarctic interior. The ^{10}Be
22 concentrations in the olivines yield minimum exposure ages (33 to 501 ka) that are
23 significantly younger than those derived from the cosmogenic ^3He (90 to 1101 ka). The
24 data reveal a complex exposure history that provide an integrated long-term erosion
25 rate of between 0.2 and 0.7 m/My that is most likely caused by mechanical weathering.
26 Inverse modelling shows that the data are readily explained by episodic erosion,

27 consisting of one to five erosion pulses that may record major regional climatic
28 changes.

29

30 *Keywords:* cosmogenic nuclides (^3He , ^{10}Be); olivine; erosion rates; episodic erosion;
31 Mount Hampton; West Antarctica

32

33 **1. Introduction**

34

35 To understand long-term landscape evolution and the role played by Cenozoic climate
36 change, it is essential to quantify the rates of erosion over different timescales (Peizhen
37 et al., 2001). The high elevation mountain tops in Antarctica have been exposed over
38 many successive glacial-interglacial cycles and are sensitive to the changing climatic
39 conditions (Sugden et al., 2005). Antarctica is the highest, driest, coldest and windiest
40 continent and records some of the lowest denudation rates (e.g., Margerison et al., 2005)
41 comparable only to the driest deserts, e.g., Atacama (Placzek et al., 2010) and South
42 Africa (Kounov et al., 2007). Consequently, the erosional record of the high altitude
43 surfaces have the potential to record climatic variations over millions of years.
44 Although climate changes affect the rate of landscape evolution, in most cases the
45 changes are averaged out into apparent steady-state erosion rates preventing
46 identification of the intrinsic dynamics of the landscape (Brunsden and Thornes, 1979).
47 Combining stable and radioactive cosmogenic nuclides has proved to be a useful
48 method to determine the complexity of landscape evolution (Balco and Shuster, 2009).

49

50 Most studies of high elevation Antarctic landscapes have combined ^{21}Ne , ^{10}Be , and ^{26}Al
51 in quartz-bearing surfaces (Van der Wateren et al., 1999; Oberholzer et al., 2003; Di

52 Nicola et al., 2009, 2012; Middleton et al., 2012; Mukhopadhyay et al., 2012). They
53 typically identify complex exposure histories that are frequently interpreted to record
54 intermittent burial beneath ice (e.g., Nishiizumi et al., 1991; Di Nicola et al., 2009,
55 2012; Mukhopadhyay et al., 2012; Hein et al. 2016; Sugden et al. 2017). In these cases
56 erosion is assumed to be in steady state, implying equilibrium between the nuclides
57 produced by cosmic radiation near the surface and the nuclide loss caused by constant-
58 surface erosion rate (Lal, 1991). Middleton et al. (2012) demonstrated how ^{26}Al - ^{10}Be -
59 ^{21}Ne data from potholes in the Dry Valleys, East Antarctica record changes in erosion
60 rate rather than burial underneath ice.

61

62 Currently, ice-free regions comprise only a few percent of the Antarctic continent, and,
63 of those, only a small proportion has been ice-free since the Miocene (Ackert et al.,
64 1999; Stone et al., 2003; Mukhopadhyay et al., 2012). The high elevation peaks (>3
65 km) in the Marie Byrd Land in West Antarctica are permanently exposed regions where
66 wind-induced ablation is more rapid than snow accumulation (Nicolas and Bromwich,
67 2014). As such, they are a key natural laboratory for the study of the erosional history
68 of the Antarctic interior.

69

70 In the first study of its kind we have developed cosmogenic ^{10}Be determination in
71 olivines and combined new data with cosmogenic ^3He measurements on the same
72 samples to unravel the erosional history of the summit of the Mount Hampton volcano
73 within the West Antarctic ice sheet (WAIS). The edifice has never been covered by a
74 significant thickness of ice and, thus, provides a simple test of the regional erosional
75 history under hyperarid climatic conditions (Rochi et al., 2006). The data reveal a
76 complex erosional history that requires long periods of extremely low erosion

77 interspersed with periods of more rapid erosion that may reflect the influence of climate
78 variations on the mechanical subaerial erosion.

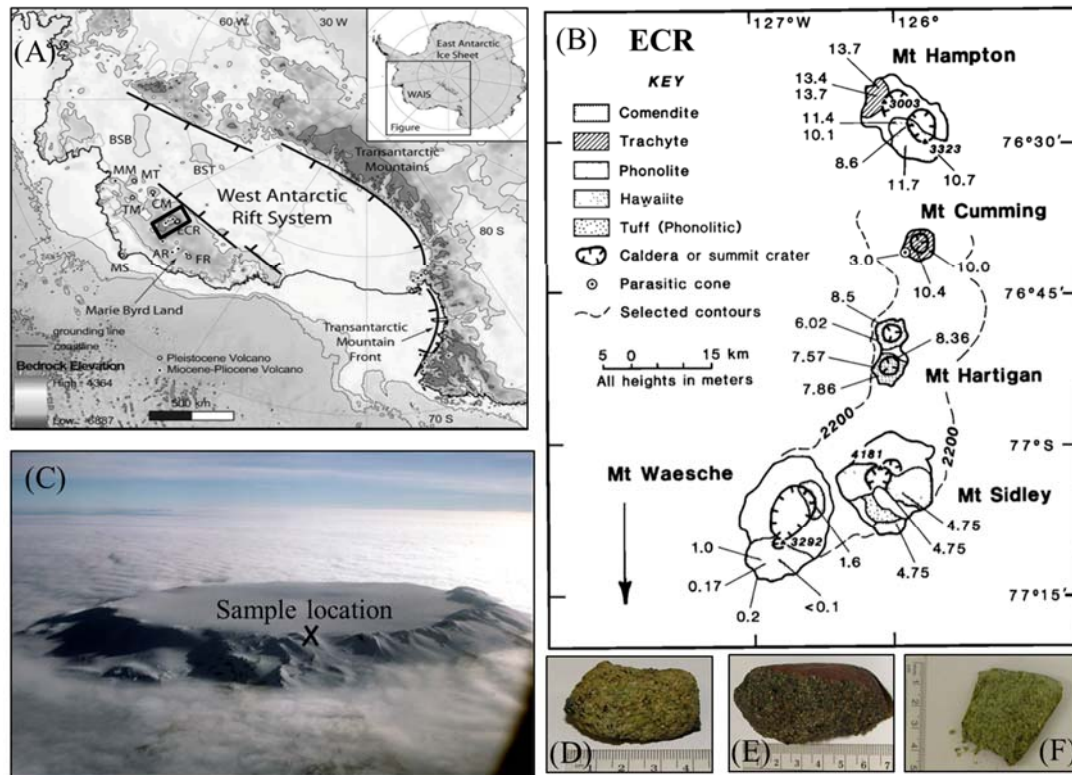
79

80 **2. Geological and glaciological context**

81

82 Mount Hampton is the northern-most volcano of 18 that protrude through the WAIS in
83 the Executive Committee Range (ECR) on the uplifted northern flank of the West
84 Antarctic Rift (Fig. 1). It is one of the oldest volcanoes in Marie Byrd Land, likely
85 produced during a peak of volcanism in the late Miocene (13.4 to 8.6 Ma; Le Masurier
86 and Rex, 1989; LeMasurier and Thomson, 1990). The summit (3323 m asl) is ~ 1000
87 m above the current WAIS surface and shows no evidence of significant erosional
88 dissection. The edifice is a symmetrical, well-preserved shield volcano with 10-15°
89 constructional slopes dominantly composed of feldspar- and augite-phyric phonolite
90 lavas (Le Masurier, 1987; LeMasurier and Thomson, 1990; Le Masurier and Rocchi,
91 2005; Rocchi et al., 2006). Crustal and lithospheric mantle xenoliths, including a suite
92 of spinel-bearing lherzolites, are found within basanites that were erupted as parasitic
93 cones close to the volcano summit (LeMasurier and Kawachi, 1990).

94



95

96 **Fig. 1.** (A) Elevation map of Antarctica showing the location of the Executive
 97 Committee Range (ECR) within Marie Byrd Land in the West Antarctic Ice Sheet
 98 interior (modified from Paulsen and Wilson, 2010). The black box represents the map
 99 in (B). (B) Geologic map of the ECR showing K-Ar ages and the sample location (red
 100 oval). This figure is modified from Le Masurier and Rex (1989). (C) Aerial view of
 101 Mount Hampton showing the sampling area for the xenoliths analysed in this study.
 102 Photograph: John Smellie. Representative xenolith samples are MH.1 (D), MH.2 (E),
 103 and MB.71.8 (F).

104

105 The surface elevation of the WAIS was at its highest at around 10 ka (Ackert et al.,
 106 1999, 2007; Anderson et al., 2002; Stone et al., 2003). The O and H isotope
 107 composition of the Byrd ice core records ice elevations that were 400 to 500 m above
 108 the current ice level during the Last Glacial Maximum (LGM) and early Holocene
 109 (Steig et al., 2001). Cosmogenic ^3He and ^{36}Cl ages of moraines from Mount Waesche
 110 in the ECR suggest that the WAIS has expanded vertically just ~ 45 m since the LGM
 111 (Ackert et al., 1999). The ^{10}Be exposure ages of glacially transported cobbles from the

112 Ford Ranges in Marie Byrd Land suggest that during the LGM the WAIS was ~700 m
113 higher than today near the coast and ~200 m higher in the interior (Stone et al., 2003).
114 A more recent study using cosmogenic ^{21}Ne and ^{10}Be from nunataks in the Ohio Range
115 on the boundary between West and East Antarctica suggest that ice thickness has not
116 been more than 160 m above current ice levels (~2200 m) since the late Miocene (~7
117 Ma) (Mukhopadhyay et al., 2012). All studies undertaken so far indicate that the highest
118 volcanic peaks of the ECR (>3000 m) have been above the ice sheet surface since their
119 eruption in the late Miocene (Ackert et al., 1999; Stone et al., 2003; Mukhopadhyay et
120 al., 2012).

121

122 **3. Sample description**

123

124 We have analysed seven lherzolite xenoliths collected from a boulder field near the
125 summit of Mount Hampton (76°30 S 125°52 W) during the second season of the
126 Antarctic expedition WAVE (West Antarctic Volcano Exploration) in January 1991.
127 The xenoliths are 4 to 8 cm diameter and were collected from within a few meters of
128 each other on the western flank. They are all likely products from the same parasitic
129 cone eruption that occurred at around 11.4 Ma (LeMasurier and Rex, 1989). The
130 xenoliths are typically composed of >50% olivine (>250 μm), ~35% orthopyroxene
131 (>250 μm), ~10% clinopyroxene (200 to 500 μm), and <2% spinel (<200 μm)
132 (Wysoczansky et al., 1995; LeMasurier et al., 2003). Electron microprobe analysis (this
133 study) reveals that the olivines from each xenolith have a near constant chemical
134 composition around Fo₉₀ and no significant compositional zonation.

135

136 **4. Analysis procedures**

137

138 *4.1. Helium isotope determinations*

139

140 The xenoliths were gently crushed, and unaltered mineral inclusion-free olivine grains
141 were handpicked from the 250-500 μm fraction under a binocular microscope. This
142 fraction was then cleaned in pure acetone ($\geq 99.8\%$) and ~ 15 mg aliquots were
143 encapsulated in Pt tubes and loaded in 21-hole Cu pans. Each sample was degassed at
144 $\sim 1400^\circ\text{C}$ using a 75 W 808 nm diode laser (Foeken et al., 2006). The magmatic helium
145 contribution was determined on ~ 1 g of olivine from xenolith MH.1 by analysis of the
146 gas released by *in vacuo* crushing using a multisample hydraulic crusher following
147 procedures in Stuart et al. (2003).

148

149 Helium concentrations and isotope compositions were measured using a *ThermoFisher*
150 Helix SFT mass spectrometer at Scottish Universities Environmental Research Centre.
151 The instrument was tuned to the maximum sensitivity following procedures
152 recommended by Burnard and Farley (2000) and Mabry et al. (2012). The instrument
153 source was operated at 4.5 kV to produce resolution >700 , reduce beam dispersion, and
154 provide the best peak shape and sensitivity (Mabry et al., 2012). The average static
155 background levels of the instrument are $1.98 \pm 0.19 \times 10^8$ and $5.0 \pm 1.9 \times 10^3$ atoms of
156 ^4He and ^3He respectively. Repeated analysis of 3×10^{12} atoms of ^4He and 9×10^7 atoms
157 of ^3He of the HESJ standard (Matsuda et al., 2002) revealed a reproducibility of 0.2%
158 and 1.1% for ^4He and ^3He measurements respectively.

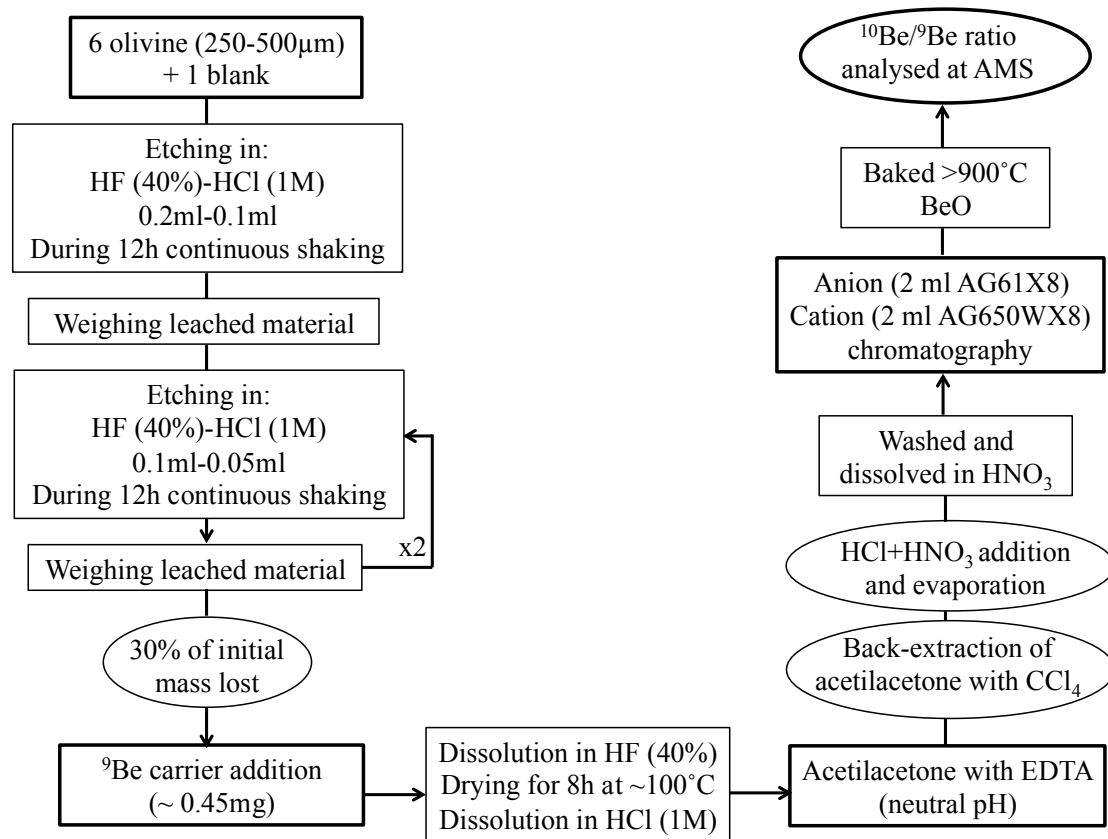
159

160 4.2. ¹⁰Be determinations

161

162 Beryllium-10 was extracted and analysed from ~1 g of olivine. Meteoric ¹⁰Be was
163 removed by three sequential HF and HCl dissolutions, that etched out >25% of the
164 initial mass. The remaining olivine was dissolved in HF and spiked with ~500 µg of
165 ⁹Be carrier (Bourlès, 1988; Brown et al., 1992). As the samples contained high amounts
166 of Mg and Fe, a procedure for isolation of Be was developed. First, a bulk Be separation
167 was performed by solvent extraction using acetyl acetone at neutral pH in the presence
168 of ethylenediaminetetra-acetic acid (EDTA) (Tabushi, 1958; Seidl, 1993; Seidl et al.,
169 1997). Beryllium was then extracted and separated by ion chromatography and
170 precipitated as BeOH using routine procedures (e.g. Child et al., 2000). The precipitate
171 was then oxidized at 800°C, mixed with 6 parts of Nb, and pressed into a Cu cathode.
172 The procedure is summarised in Fig. 2. The ¹⁰Be/⁹Be ratios of the six samples and the
173 blank were measured using the 5 MV NEC Pelletron accelerator mass spectrometer at
174 SUERC (Xu et al., 2010). The ¹⁰Be concentrations are based on a ¹⁰Be/⁹Be ratio of 2.79
175 x 10⁻¹¹ for NIST Standard Reference Material 4325. The data have been corrected with
176 a procedural blank (representing 0.4 to 6% of the total ¹⁰Be measured).

177



178

179 **Fig. 2.** Schematic representation of the procedures followed for ^{10}Be isolation from
180 olivine.

181

182 4.3. Production rates

183

184 The production rates used for exposure age and erosion rate calculations from the
185 measured cosmogenic ^3He and ^{10}Be concentrations are scaled for latitude ($76^{\circ}30'\text{S}$,
186 $125^{\circ}52'\text{W}$) and elevation (3020 m) using Lal (1991)/Stone (2000) scaling factors and
187 following the scheme implemented by Balco et al. (2008) for ^{10}Be and Marrero et al.
188 (2016) for ^3He . The SLHL production rate for ^3He is taken from Goehring et al. (2010)
189 and ^{10}Be is taken from Borchers et al. (2016). The production rates are scaled for
190 composition using production ratios obtained from the element-specific production
191 rates of Masarik (2002). To calculate the theoretical erosion rates, we applied inverse
192 modelling using a convergent Monte-Carlo approach based on the equations from Lal

193 (1991), detailed explanation of the calculations, and parameters used for modelling are
 194 provided in section 6.2.

195

196 **5. Results**

197

198 The ^3He concentrations and $^3\text{He}/^4\text{He}$ ratios are reported in Table 1. The ^3He
 199 concentrations in the melt steps vary from 1.5 to 18.9×10^8 atoms/g and $^3\text{He}/^4\text{He}$ ratios
 200 range from 24 to 11,543 R_a , where R_a is the isotope composition of He in air ($1.39 \times$
 201 10^{-6}). Multiple aliquots of olivine from each xenolith were measured. Helium was
 202 measured in nine aliquots of olivine from xenolith MH.2 in an effort to fully determine
 203 the data quality. The $\pm 5\%$ uncertainty in the average ^3He concentration is beyond the
 204 reproducibility determined from HESJ. This overdispersion is unlikely to represent
 205 variation in other He sources (see below) and may reflect weighing errors and subtle
 206 variation in cosmogenic He production within the xenolith.

207

208 **Table 1**

209 Helium isotope data from olivine separates from Mount Hampton xenoliths

Sample	Weight (mg)	^3He (10^8 atoms/g)	1σ	$^3\text{He}/^4\text{He}$ (R_a)	1σ
MH.1	9.7	15.77	0.19	8429	198
MH.1	11.2	15.73	0.19	1525	1
Average		15.75	0.03		
MH.2	12.0	8.43	0.14	211	4
MH.2	13.5	8.27	0.15	1469	33
MH.2	12.1	7.44	0.12	5849	156
MH.2	14.0	7.96	0.11	4902	101
MH.2	12.2	7.68	0.13	5001	157
MH.2	14.9	7.62	0.12	10693	245
MH.2	15.0	7.65	0.12	11543	279
MH.2	11.3	8.52	0.15	3523	56
MH.2	16.6	7.91	0.13	2330	48
Average		7.94	0.39		
MB.71.7	13.7	1.79	0.05	24	1
MB.71.7	9.5	1.77	0.06	134	5
Average		1.78	0.01		
MB.71.8	12.3	18.94	0.21	2524	345
MB.71.8	16.4	18.67	0.19	1126	18

Average		18.81	0.19		
MB.71.9	18.0	5.26	0.09	432	9
MB.71.9	12.9	5.13	0.08	543	11
MB.71.9	14.9	5.68	0.09	396	8
MB.71.9	12.4	5.40	0.11	174	4
Average		5.37	0.24		
MB.71.10	13.4	1.56	0.05	783	30
MB.71.10	8.0	1.53	0.06	35	2
MB.71.10	12.6	1.47	0.04	63	2
MB.71.10	10.6	1.46	0.04	449	14
Average		1.51	0.05		

210

211 Determining the cosmogenic He concentration in old volcanic rocks requires that the
212 inventories of nucleogenic-radiogenic and magmatic He are quantified (Margerison et
213 al., 2005; Williams et al., 2005). The $^3\text{He}/^4\text{He}$ ratio of nucleogenic-radiogenic He
214 produced in olivine is low, approaching the canonical value of crustal radiogenic He
215 ($<0.05 R_a$), reflecting the low Li content (Ryan and Kyle, 2004; Seitz et al., 2004). The
216 high measured $^3\text{He}/^4\text{He}$ ratios of the Mount Hampton olivines ($>24 R_a$) imply that the
217 contribution of nucleogenic ^3He is negligible.

218

219 *In vacuo* crushing extracts magmatic He by rupturing melt/vapour inclusions (e.g.,
220 Stuart et al., 1995). Sample MH.1 released $2.8 \pm 0.8 \times 10^5$ atoms $^3\text{He}/\text{g}$, yielding a
221 $^3\text{He}/^4\text{He}$ ratio of $9.02 \pm 1.64 R_a$ (1σ). Panter et al. (2000) characterized the basalts from
222 the Marie Byrd Land as having a strong high μ (HIMU) signature with no evidence of
223 crustal contamination. If the $^3\text{He}/^4\text{He}$ ratio of HIMU-influenced mantle is $6.5 \pm 0.6 R_a$
224 (Parai et al., 2009, and references therein), a small contribution of cosmogenic He has
225 been released by crushing. The cosmogenic ^3He released by crushing ($8.2 \pm 4.1 \times 10^4$
226 atoms/g) represents $<0.05\%$ of the total of the sample with least $^3\text{He}_{\text{cos}}$ (see below),
227 demonstrating that the *in vacuo* crushing method employed here does not release a
228 significant proportion of the cosmogenic ^3He in olivine.

229

230 The concentration of magmatic ^3He ($^3\text{He}_{\text{magmatic}}$) released by crushing can be calculated
231 from the following relationship:

232

$$233 \quad ^3\text{He}_{\text{magmatic}} = ^3\text{He}_{\text{crush}} \times (^3\text{He}/^4\text{He}_{\text{magmatic}}/{}^3\text{He}/^4\text{He}_{\text{crush}}) \quad (1)$$

234

235 where the subscript crush refers to He released by *in vacuo* crushing. The magmatic
236 ^3He released in this experiment (1.98×10^5 atoms/g) represents <0.1% of the total ^3He
237 released by melting the Mount Hampton olivines. Thus, it can be neglected, implying
238 that all the ^3He released by degassing all samples can be considered to be cosmogenic
239 in origin.

240

241 The minimum exposure ages calculated from the average cosmogenic ^3He
242 concentrations in each sample range from 90 to 1101 ka (Table 2). These correspond
243 to steady-state erosion rates of 0.45 to 5.51 m/Ma (Table 2).

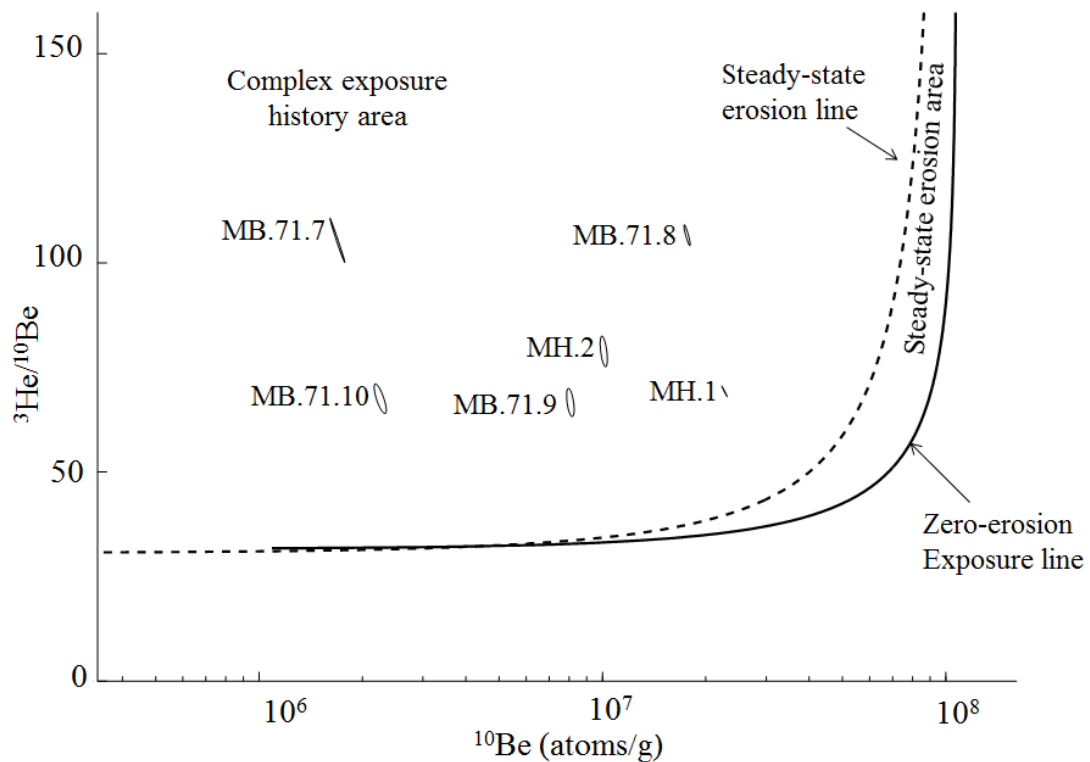
244

245 The ^{10}Be concentrations in the Mount Hampton olivines vary from 0.17 to 2.27×10^7
246 atoms/g (Table 2). These correspond to minimum exposure ages of between 33 and 501
247 ka and maximum erosion rates of 1.2 to 19.7 m/Ma (Table 2). The minimum exposure
248 ages are systematically younger than those derived from cosmogenic ^3He , and the
249 apparent erosion rates are higher.

250

251 The $^3\text{He}/^{10}\text{Be}$ ratios vary from 66.5 to 106.6. These are more than twice the
252 instantaneous production ratio in olivine (~ 30). The data plot within the area of complex
253 exposure on a $^3\text{He}/^{10}\text{Be}$ vs. ^{10}Be diagram (Fig. 3) rules out the possibility that they record
254 long-term steady-state erosion. The ^3He - ^{10}Be data require either a complex history of

255 exposure, burial and reexposure, or pervasive nonsteady state (i.e., variable) erosion
 256 (Lal, 1991).



257
 258 **Fig. 3.** Plot of ^{10}Be concentration vs. $^3\text{He}/^{10}\text{Be}$ for Mount Hampton xenolith olivine.
 259 Ellipses represent the 68% confidence interval. The banana-shaped area is the steady-
 260 state erosion area (Lal, 1991). The continuous line represents the evolution of the
 261 $^3\text{He}/^{10}\text{Be}$ ratio with time in a surface that has experienced zero erosion. The dotted line
 262 represents the $^3\text{He}/^{10}\text{Be}$ ratio generated by steady-state erosion of at least one mean
 263 cosmic ray attenuation length at a constant rate for infinite amount of time.

Table 264

Compilation of the data of ^{10}Be and ^3He from olivine separates from xenoliths from Mount Hampton

Sample	Latitude S	Longitude W	Elevation (m)	Olivine (Fo)	^{10}Be (10^7 atoms/g)	1σ	^{10}Be Apparent erosion rate (m/Ma)	1σ	PR ^{10}Be _Qtz scaled with Lal(1991)/Stone (2000)	N factor	^{10}Be Apparent exposure age (ka)	1σ	^3He average (10^8 atoms/g)	1σ	^3He Apparent erosion rate (m/Ma)	1σ	PR ^3He _Fo ₈₄ scaled to Lal(1991)/Stone (2000)	N factor	^3He Apparent exposure age (ka)	1σ	$^3\text{He}/^{10}\text{Be}$	1σ
MH.1	76° 30'	125° 52'	3020	91	2.27	0.04	1.18	0.77	51.92	0.884	501	40	15.75	0.03	0.53	0.08	1674.0289	1.031	925	140	69.43	1.29
MH.2	76° 30'	125° 52'	3020	91	1.01	0.02	3.01	1.75	51.92	0.883	208	16	7.94	0.39	1.05	0.16	1674.0289	1.030	467	74	78.79	3.66
MB.71.7	76° 30'	125° 52'	3020	91	0.17	0.01	19.70	2.49	51.92	0.883	33	3	1.78	0.01	4.70	0.71	1674.0289	1.030	104	16	105.26	5.29
MB.71.8	76° 30'	125° 52'	3020	91	1.76	0.04	1.60	0.99	51.92	0.883	379	30	18.81	0.19	0.45	0.07	1674.0289	1.031	1101	170	106.60	2.47
MB.71.9	76° 30'	125° 52'	3020	89	0.81	0.02	3.85	2.19	51.92	0.875	165	13	5.37	0.24	1.56	0.25	1674.0289	1.029	319	51	66.53	3.38
MB.71.10	76° 30'	125° 52'	3020	90	0.23	0.01	14.68	1.80	51.92	0.877	46	4	1.51	0.05	5.51	0.85	1674.0289	1.030	90	14	67.41	3.52

The scaled production rates of ^{10}Be and ^3He are calculated using the CRONUS calculators v. 2.3 (Balco et al., 2008) version 2.3 and Marrero et al. (2016)

respectively. The Normalization factor (N) accounts for composition using production ratios obtained from the element-specific production rates of Masarik

(2002). Apparent exposure ages are calculated following the equations of Lal (1991), assuming zero erosion.

269 **6. Discussion**

270 *6.1 Intermittent burial*

271

272 The Mount Hampton edifice has never been covered by the WAIS (see section 2), and
273 the summit shows no geomorphic features that are indicative of the accumulation of
274 significant wet-based ice, such as striated, polished, or ice-moulded rock surfaces (Le
275 Masurier, 1987; Le Masurier and Rocchi, 2005; Rocchi et al., 2006). Complete
276 cessation of the production of cosmogenic He and Be requires the local accumulation
277 of ~ 10 m of cold-based ice. The high elevation and location deep within Marie Byrd
278 Land interior far from coastal areas of high snow precipitation strongly restricts ice
279 accumulation. Marie Byrd Land is the only Antarctic region where the mean katabatic
280 flow has a strong southward component, causing a precipitation shadow effect over the
281 ECR and producing a strong foehn wind effect that causes the snowfall to
282 sublimate/evaporate (Nicolas and Bromwich, 2014). Therefore, it is unlikely that a
283 sizeable ice cap has ever existed for any significant period of time, meaning that
284 intermittent burial caused by a waxing and waning of semipersistent ice cover is
285 implausible.

286

287 Volcanic activity at Mount Hampton ceased at 8.6 Ma and migrated southward along
288 the ECR (LeMasurier and Rex, 1989), and no field evidence of tephra deposits near the
289 sample site was observed. This rules out burial beneath intermittent volcanic deposits
290 as an explanation for the ^3He - ^{10}Be data.

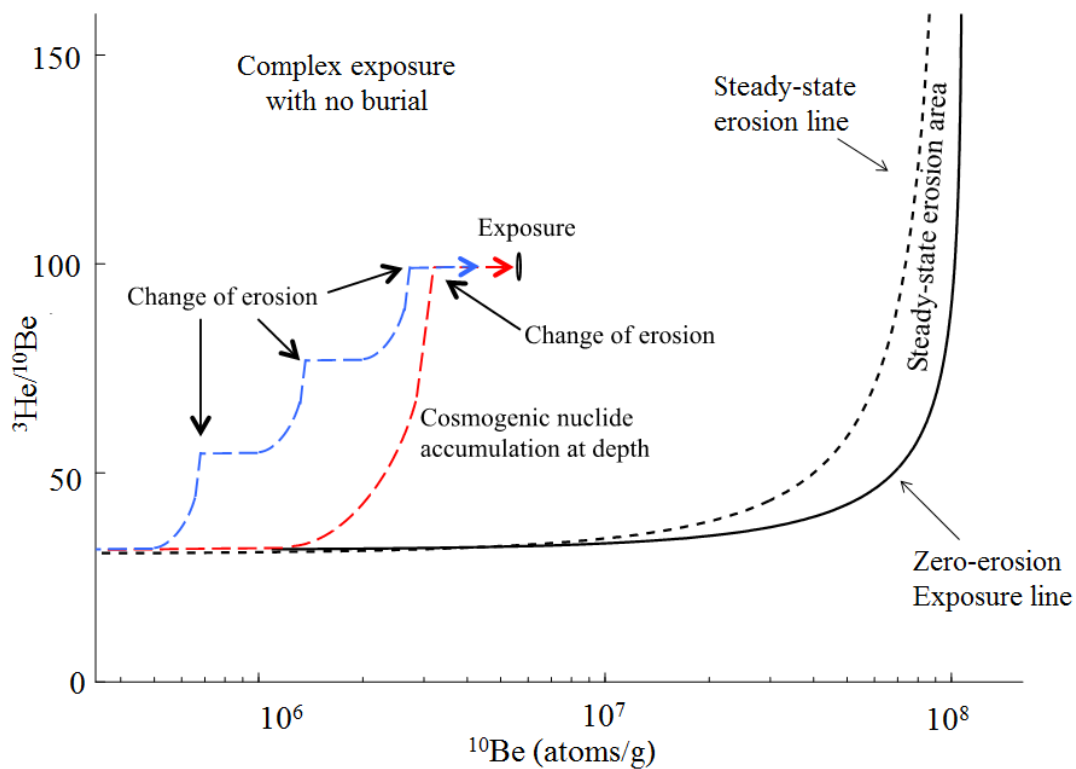
291

292 6.2 Erosion rate variation

293

294 Lal (1991) noted that nonsteady state erosion, i.e., changing erosion rates, generates
295 cosmogenic nuclide ratios that plot in the complex exposure zone. Kober et al. (2007)
296 and Middleton et al. (2012) also considered the possibility of episodic erosion being
297 the cause of the nonsteady state cosmogenic ^{21}Ne - ^{10}Be - ^{26}Al signatures in northern Chile
298 and Antarctica respectively. The evolution of the $^3\text{He}/^{10}\text{Be}$ ratio during nonsteady state
299 erosion is shown in Fig. 4.

300

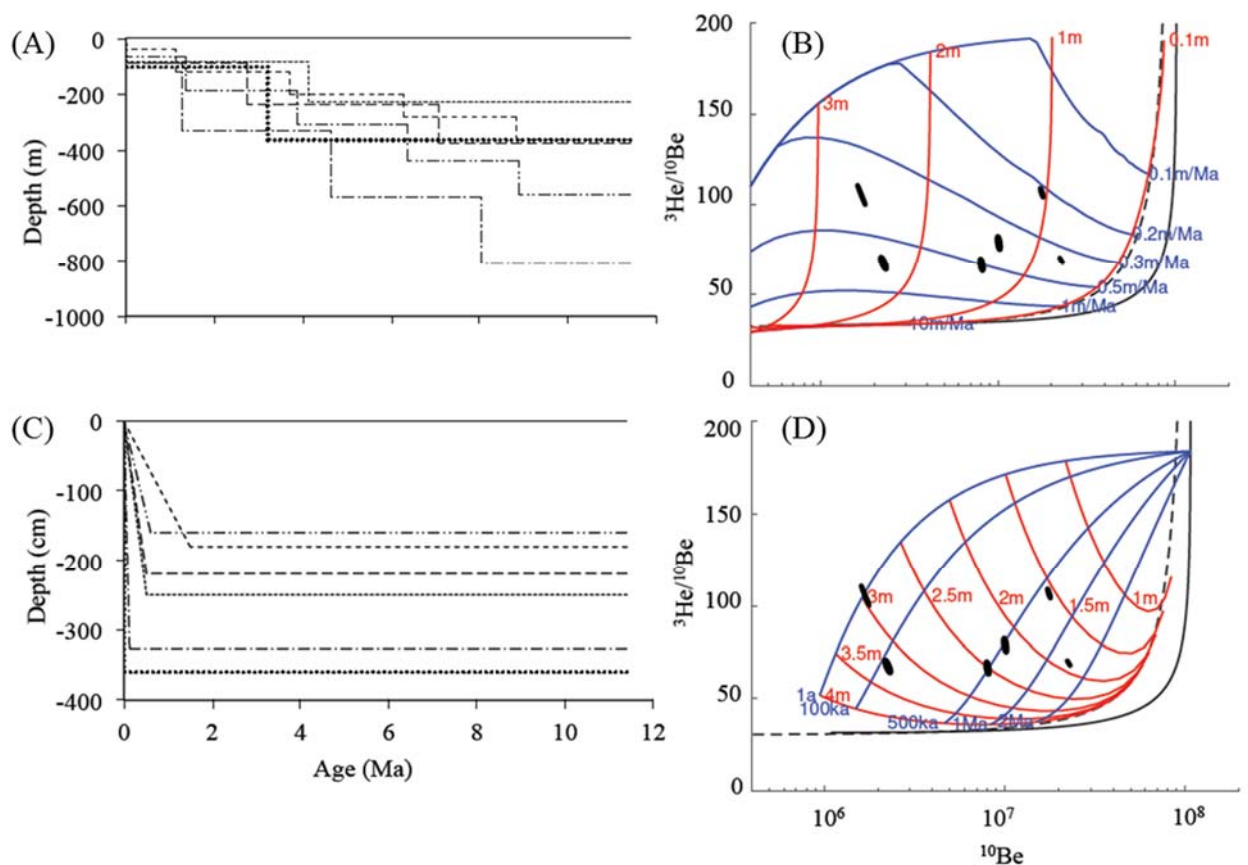


301

302 **Fig. 4.** Schematic representation of the evolution of cosmogenic $^3\text{He}/^{10}\text{Be}$ ratio under
303 conditions of episodic erosion consisting on several (blue) or one (red) erosion pulses
304 to generate signatures that fall on the complex exposure area of the ^{10}Be vs. $^3\text{He}/^{10}\text{Be}$
305 diagram.

306

307 To quantify the timescale and magnitude of episodic erosional events and the duration
 308 of the final stage of complete exposure that satisfies the Mount Hampton xenolith He-
 309 Be data, we have modelled two extreme nonsteady-state erosion scenarios. Model 1
 310 considers multiple erosional pulses that are assumed to last an equal length of time.
 311 This is shown schematically in Fig. 5A. In this model the integrated erosion rate is the
 312 average over the period since eruption. Model 2 considers the possibility of a single
 313 erosion pulse in the Pleistocene that brought all the xenoliths to the surface from
 314 different depths. This model assumes that the erosion rate was negligible prior to the
 315 erosion pulse and is shown schematically in Fig. 5C. Figs. 5B and 5D show the
 316 evolution of $^3\text{He}/^{10}\text{Be}$ and ^{10}Be concentrations in the olivines for the two scenarios.
 317 Table 3 summarises the parameters and variables used to generate the two models.
 318



319

320 **Fig. 5.** Two models to explain the cosmogenic ^3He and ^{10}Be data from Mount Hampton
321 xenolith olivine. **(A)** and **(C)** are schematic representations of model 1 and model 2
322 respectively (see text) showing the episodic erosion of several xenoliths (dashed lines)
323 on their way to the surface (continuous line). **(B)** Plot of the output of model 1. The red
324 lines represent the amount of material removed in a single erosional event, and the blue
325 lines record the average erosion rate over 11.4 Ma. The lines have been determined
326 using Eqs. (2) and (3) (see text). The grey continuous and discontinuous lines represent
327 the steady-state erosion area (Lal, 1991; Balco et al., 2008). **(D)** Output of model 2.

Table 3

Summary of the parameters used to model the cosmogenic ^3He and ^{10}Be data from Mount Hampton xenolith olivine.

Model parameters	Values	Notes and references ^a
General parameters^b		
^{10}Be production rate for olivine (FO_{89-91}) at Mount Hampton	45.9 atoms/g/y	Following the scheme of CRONUS calculators Matlab code v 2.3 Balco et al. (2008) scaling factor Lal (1991)/Stone (2000) scaled for composition using Masarik (2002)
^3He production in olivine (FO_{89-91}) at Mount Hampton	1725 atoms/g/y	Following the scheme of Marrero et al. (2016) scaling factor Lal (1991)/Stone (2000) scaled for composition using Masarik (2002)
Production rate from fast muons	0.0777 atoms/g/y	Calculated using CRONUS calculators Matlab code v 2.3 Balco et al. (2008)
Production rate from negative muon capture	0.0992 atoms/g/y	
Attenuation length from neutron spallation	160 g/cm ²	Balco et al. (2008); Gosse and Phillips (2001)
Attenuation length from fast muons	2.60 x 10 ³ g/cm ²	Calculated using CRONUS calculators Matlab code v 2.3 Balco et al. (2008)
Attenuation length from negative muon capture	1.30 x 10 ³ g/cm ³	Calculated using CRONUS calculators Matlab code v 2.3 Balco et al. (2008)
Half-life for ^{10}Be	1.378 Ma	Chmeleff et al. (2010); Korschinek et al. (2010)
Rock density	2.67 g/cm ³	
Constant exposure-erosion lines		Calculated applying equations from Lal (1991) for constant exposure at zero erosion and for steady-state erosion for infinite time
Model 1		
Average erosion rate (m/Ma)		Episodic erosion. Material is removed in steps Erosion rate is taken as an average for the total residence time (11.4Ma)
Material removed from one erosive event (m)		Erosive events are assumed to last an equal length of time
Total duration of complex history	11.4 Ma	Le Masurier and Rex (1989)
Model 2		
Accumulation depth (m)		Single erosion pulse. Erosion rate is assumed to be zero during the time of accumulation at depth prior to the removal of material Material removed to place the samples at the surface
Time when erosion started		This considers the time at depth required to generate the ^3He - ^{10}Be signature including a time of erosion
Total duration of complex history	11.4 Ma	Le Masurier and Rex (1989)

^aReferences for the chosen values are listed where applicable. All the parameters have been calculated using the equations of Lal (1991) modified by Balco et al. (2008) to include muon production. The models have been calculated using Matlab coding.

^bParameters of complex exposure common to all the models.

335

336 Both models start at 11.4 Ma based on the K-Ar age of Mt. Hampton phonolites

337 (LeMasurier and Rex, 1989). The production of cosmogenic ^3He and ^{10}Be have been

338 calculated according to

339

$$340 \quad {}^3He = \frac{P_{3sp}}{\frac{\varepsilon\rho}{\Lambda sp}} \left(e^{-\frac{z\rho}{\Lambda sp}} \right) \left(1 - e^{-\left(\frac{\varepsilon\rho}{\Lambda sp}\right)T} \right) \quad (2)$$

$$341 \quad {}^{10}Be = \frac{P_{10sp}}{\lambda_{10} + \frac{\varepsilon\rho}{\Lambda sp}} \left(e^{-\frac{z\rho}{\Lambda sp}} \right) \left(1 - e^{-\left(\lambda_{10} + \frac{\varepsilon\rho}{\Lambda sp}\right)T} \right) + \frac{P_{10fm}}{\lambda_{10} + \frac{\varepsilon\rho}{\Lambda fm}} \\ 342 \quad \left(e^{-\frac{z\rho}{\Lambda fm}} \right) \left(1 - e^{-\left(\lambda_{10} + \frac{\varepsilon\rho}{\Lambda fm}\right)T} \right) + \frac{P_{10sm}}{\lambda_{10} + \frac{\varepsilon\rho}{\Lambda sm}} \left(e^{-\frac{z\rho}{\Lambda sm}} \right) \left(1 - e^{-\left(\lambda_{10} + \frac{\varepsilon\rho}{\Lambda sm}\right)T} \right) \quad (3)$$

343

344 where P_{3sp} and P_{10sp} are the production rates of 3He and ${}^{10}Be$ by spallation of fast
345 neutrons; P_{10fm} and P_{10sm} are the ${}^{10}Be$ production rates by neutron spallation, fast muon
346 radiation, and negative muon radiation; ε is the erosion rate; ρ is the density of the rock;
347 λ_{10} is the decay constant of ${}^{10}Be$; and $\Lambda_{sp, fm, sm}$ are the respective attenuation lengths with
348 depth z (Lal, 1991; Gosse and Phillips, 2001; Balco et al., 2008). Muon interactions
349 account for nearly all the cosmogenic Be production at a few meters below the surface.
350 Cosmogenic 3He is not produced significantly by muon radiation and is assumed to be
351 negligible in this case.

352

353 The models are sensitive to variations in the ${}^3He/{}^{10}Be$ ratios rather than in the individual
354 production rates. The effects of self-shielding and from snow cover have been
355 considered. Assuming 1 m of continuous snow coverage and an average size of the
356 xenoliths of 4 cm, the ${}^3He/{}^{10}Be$ ratios vary by 0.25% having no effect on the
357 interpretation of the models.

358

359 The values of the model parameters that fit the sample 3He and ${}^{10}Be$ concentrations
360 were calculated by inverse modelling using a convergent Monte-Carlo approach. The
361 parameters that satisfy the pulsed erosion model (model 1) are summarized in Table 4.

362 The data can be explained by between two and five erosion pulses that have removed

363 between 0.8 and 2.6 m of overburden. Thus, the long-term erosion rates range from
 364 0.20 to 0.71 m/My. Erosion rates of this magnitude are typical of high elevation
 365 landscapes in the Antarctic (e.g., Marrero et al., 2018, and references therein).

366

367 **Table 4**

368 Summary of the minimum amount of material removed and maximum erosion rates (ϵ)
 369 required to generate the cosmogenic ^3He - ^{10}Be signatures; the total material removed
 370 over 11.4 Ma and the minimum number of events necessary to remove this material has
 371 been calculated (uncertainties are reported as 1σ).

Sample name	Material removed in one event (m)	\pm	ϵ (m/Ma) over 11.4Ma	\pm	Total material removed (m)	\pm	n. events	\pm
MH.1	0.82	0.07	0.32	0.03	3.65	0.34	4.4	0.6
MH.2	1.43	0.11	0.33	0.03	3.76	0.34	2.6	0.3
MB.71.7	2.62	0.21	0.32	0.03	3.65	0.34	1.4	0.2
MB.71.8	1.23	0.10	0.49	0.04	5.59	0.46	4.5	0.5
MB.71.9	1.45	0.12	0.20	0.02	2.28	0.23	1.6	0.2
MB.71.10	2.4	0.19	0.71	0.06	8.09	0.68	3.4	0.4

372

373 For the single erosional event model (model 2), the minimum depths at which the
 374 samples could have resided and the maximum time for the erosion rate change have
 375 been determined. Table 5 summarises the results obtained by inverse modelling. The
 376 cosmogenic ^3He - ^{10}Be data require that the xenoliths have spent most of the time since
 377 eruption at between 1.6 and 3.0 m below the surface, followed by a pulse of erosion of
 378 between 1.2 to 306 m/Ma starting at 1.5 Ma. This model records the maximum amount
 379 of material removed in a minimum time with erosion able to remove up to 3.3 m in a
 380 short period of time (~ 10 ka). In this model, the data require a long-term average erosion
 381 rate that is <1 m/My.

382

383 **Table 5**

384 Summary of the minimum depth at which samples have been accumulating cosmogenic
 385 nuclides and apparent erosion rates (ϵ) over a maximum time (time of removal) required
 386 for generating the cosmogenic ^3He - ^{10}Be data (uncertainties are reported as 1σ).

Sample name	Depth (m)	±	Time of removal (Ma)	±	Apparent short-term ϵ (m/Ma)	±
MH.1	1.80	0.14	1.50	0.12	1.20	0.14
MH.2	2.20	0.18	0.50	0.04	4.40	0.50
MB.71.7	3.06	0.24	0.01	0.00	306.00	34.6
MB.71.8	1.60	0.13	0.60	0.05	2.67	0.30
MB.71.9	2.50	0.20	0.50	0.04	5.00	0.57
MB.71.10	3.27	0.26	0.11	0.01	29.70	3.40

387

388 Erosion rate increases mainly occur during changes from periods of stability to times
389 of frequent abrupt changes in temperature and precipitation that break the landscape
390 equilibrium (Peizhen et al., 2001). Since the late Miocene several glacial-interglacial
391 cycles have been responsible for fluctuations in the climatic conditions in Antarctica
392 that might have resulted in episodic erosion rate changes that average out into low long-
393 term erosion rates that are typical of the region. The multiple erosional pulses required
394 in model 1 may record major climatic changes such as the transition from cool to
395 warmer climatic conditions during the late Pliocene, Quaternary cooling, or middle
396 Pleistocene warming (Pollard and DeConto, 2009). The major Pleistocene erosion
397 pulse tracked in model 2 that brought the xenoliths to the surface may correspond to
398 the transition to cooler climatic conditions during the late Pleistocene (Raymo et al.,
399 2006).

400

401 The xenoliths in this study are from a block field of loose volcanic material typical of
402 the exposed mountain tops above the WAIS. Such surfaces are more susceptible to
403 erosion and weathering than those that have experienced ice cover (Sudgen et al., 2005)
404 and therefore are more sensitive to the instability generated by changing climate.
405 Physical rock weathering is responsible for rock mass loss under wet or dry conditions
406 in the case of the extreme low Antarctic temperatures (Elliot, 2008). Andrews and Le
407 Masurier (1973) observed water accumulation produced by local snowmelt during the

408 Antarctic summers. This could be responsible for local freeze-thaw type erosion, which
409 would comminute rock slabs with consequent increase in the short-term erosion rates.

410

411 **7. Conclusions**

412

413 We have developed a procedure for the extraction and measurement of cosmogenic
414 ^{10}Be from olivine. By combining ^{10}Be with cosmogenic ^3He determinations from
415 olivine we can resolve the complexity of long-term landscape development in
416 Antarctica using the volcanic edifices that protrude through the West Antarctic Ice
417 Sheet. Data from mantle xenolith from the summit of Mount Hampton volcano in
418 Marie Byrd Land reveal the episodic erosional history, integrated over an average
419 long-term erosion rate of <1 m/Ma, which is within the range recorded by long-term
420 Antarctica. The data are consistent with an increase of erosion rate, to 2 m/Ma for the
421 last 1.5 Ma or several episodes of erosion that have removed up to ~ 2.6 m of material
422 over the last 11.4 Ma. Further resolution of the complexity of the erosional history
423 awaits development of other cosmogenic chronometers (e.g., ^{36}Cl)

424

425 Our study has empirically demonstrated the episodic nature of surface erosion at a high-
426 latitude, high-elevation site in interior Antarctica and that changes in erosion regime
427 can generate cosmogenic nuclide signatures that plot within the complex exposure area
428 on a two-isotope diagram with no need for cycles of exposure-burial-reexposure. This
429 interpretation is rarely considered when interpreting complex ^{26}Al ^{10}Be - ^{21}Ne
430 systematics of Antarctic surfaces. Complex exposure caused by erosion rate variations
431 is a viable alternative explanation for complex exposure-related isotopic signatures and
432 therefore should be considered especially in the cases in which no clear evidence of ice

433 cover is observed. Why and how climate change drove the erosion rate increases is still
434 unclear, but our study strongly suggests that the application of multiple cosmogenic
435 nuclides have a clear potential to trace past environmental or climatic changes in arid
436 regions.

437

438 **Acknowledgements**

439 The PhD of AC was supported by NERC and SUERC. We thank Prof. John Gamble
440 for providing some of the Mount Hampton xenoliths and Dr. Luigia Di Nicola for her
441 valuable assistance in the laboratory and in data interpretation. We also thank the
442 reviewers and the editor for their help improving the manuscript.

443

444 **References**

- 445 Ackert, R.P., Barclay, D.J., Borns, H.W., Calkin, P.E., Kurz, M.D., Fastook, J.L., Steig,
446 E.J., 1999. Measurements of past ice sheet elevations in interior West Antarctica.
447 *Science* 286(5438), 276-280.
- 448 Ackert, R.P., Mukhopadhyay, S., Parizek, B.R., Borns, H.W., 2007. Ice elevation near
449 the West Antarctic Ice Sheet divide during the last glaciation. *Geophysical Research*
450 *Letters* 34(21) L21506.
- 451 Anderson, J.B., Shipp, S.S., Lowe, A.L., Wellner, J.S., Mosola, A.B., 2002. The
452 Antarctic Ice Sheet during the Last Glacial Maximum and its subsequent retreat
453 history: a review. *Quaternary Science Reviews* 21(1), 49-70.
- 454 Andrews, J.T., LeMasurier, W.E. (1973). Rates of Quaternary glacial erosion and corrie
455 formation, Marie Byrd Land, Antarctica. *Geology* 1(2), 75-80.
- 456 Balco, G., Shuster, D.L., 2009. ^{26}Al - ^{10}Be - ^{21}Ne burial dating. *Earth and Planetary*
457 *Science Letters* 286(3), 570-575.
- 458 Balco, G., Stone, J.O., Lifton, N.A., Dunai, T.J., 2008. A complete and easily accessible
459 means of calculating surface exposure ages or erosion rates from ^{10}Be and ^{26}Al
460 measurements. *Quaternary geochronology* 3(3), 174-195.
- 461 Borchers, B., Marrero, S., Balco, G., Caffee, M., Goehring, B., Lifton, N., Stone, J.,
462 2016. Geological calibration of spallation production rates in the CRONUS-Earth
463 project. *Quaternary Geochronology* 31, 188-198.
- 464 Bourlès, D., 1988. Étude de la géochimie de l'isotope cosmogénique ^{10}Be et de son
465 isotope stable ^9Be en milieu océanique: application à la datation des sédiments
466 marins. Ph.D. dissertation, Paris-sud Centre d'Orsay.
- 467 Brown, E.T., Brook, E.J., Raisbeckl, G.M., Yioul, F., Kurz, M.D., 1992. ^{10}Be and ^{26}Al
468 in quartz: implications for exposure age dating. *Geophysical Research Letters* 19(4),
469 369-372.

- 470 Brunsdon, D., Thornes, J.B. (1979). Landscape sensitivity and change. Transactions of
471 the Institute of British Geographers 463-484.
- 472 Burnard, P. G., Farley, K. A., 2000. Calibration of pressure - dependent sensitivity and
473 discrimination in Nier-type noble gas ion sources. *Geochemistry, Geophysics,*
474 *Geosystems* 1(7) (2000GC00038).
- 475 Child, D., Elliott, G., Mifsud, C., Smith, A. M., Fink, D., 2000. Sample processing for
476 earth science studies at ANTARES. *Nuclear Instruments and Methods in Physics*
477 *Research Section B: Beam Interactions with Materials and Atoms* 172(1-4), 856-
478 860.
- 479 Chmeleff, J., von Blanckenburg, F., Kossert, K., Jakob, D., 2010. Determination of the
480 ^{10}Be half-life by multi-collector ICP-MS and liquid scintillation counting. *Nuclear*
481 *Instruments and Methods in Physics Research Section B: Beam Interactions with*
482 *Materials and Atoms* 268(2), 192-199.
- 483 Di Nicola, L., Strasky, S., Schlüchter, C., Salvatore, M.C., Akçar, N., Kubik, P.W.,
484 Christl, M., Kasper, H.U., Wieler, R., Baroni, C., 2009. Multiple cosmogenic
485 nuclides document complex Pleistocene exposure history of glacial drifts in Terra
486 Nova Bay (northern Victoria Land, Antarctica). *Quaternary Research* 71(1), 83-92.
- 487 Di Nicola, L., Baroni, C., Strasky, S., Salvatore, M.C., Schlüchter, C., Akçar, N.,
488 Kubik, P.W., Wieler, R., 2012. Multiple cosmogenic nuclides document the stability
489 of the East Antarctic Ice Sheet in northern Victoria Land since the Late Miocene (5–
490 7 Ma). *Quaternary Science Reviews* 57, 85-94.
- 491 Elliott, C., 2008. Influence of temperature and moisture availability on physical rock
492 weathering along the Victoria Land coast, Antarctica. *Antarctic Science* 20(1), 61-
493 67.
- 494 Foeken, J.P.T., Stuart, F.M., Dobson, K.J., Persano, C., Vilbert, D., 2006. A diode laser
495 system for heating minerals for (U-Th)/He chronometry. *Geochemistry Geophysics*
496 *Geosystems*. 7, Q04015, doi:10.1029/2005GC001190.
- 497 Goehring, B.M., Kurz, M.D., Balco, G., Schaefer, J.M., Licciardi, J., Lifton, N., 2010.
498 A reevaluation of in situ cosmogenic ^3He production rates. *Quaternary*
499 *Geochronology* 5(4), 410-418.
- 500 Gosse, J.C., Phillips, F.M., 2001. Terrestrial in situ cosmogenic nuclides: theory and
501 application. *Quaternary Science Reviews* 20(14), 1475-1560.
- 502 Hein, A.S., Woodward, J., Marrero, S.M., Dunning, S.A., Freeman, S., Stuart, F.M.,
503 Winter, S., Westoby, M.J., Sugden, D.E. 2016. Evidence for dynamic equilibrium
504 of the central divide of the West Antarctic Ice Sheet for 1.4 million years. *Nature*
505 *Communications* 10.1038/NCOMMS10325.
- 506 Kober, F., Ivy-Ochs, S., Schlunegger, F., Baur, H., Kubik, P.W., Wieler, R. 2007.
507 Denudation rates and a topography-driven rainfall threshold in northern Chile:
508 Multiple cosmogenic nuclide data and sediment yield budgets. *Geomorphology*
509 83(1-2), 97-120.
- 510 Korschinek, G., Bergmaier, A., Faestermann, T., Gerstmann, U.C., Knie, K., Rugel, G.,
511 Kossert, K., 2010. A new value for the half-life of ^{10}Be by heavy-ion elastic recoil
512 detection and liquid scintillation counting. *Nuclear Instruments and Methods in*
513 *Physics Research Section B: Beam Interactions with Materials and Atoms* 268(2),
514 187-191.
- 515 Kounov, A., Niedermann, S., De Wit, M.J., Viola, G., Andreoli, M., Erzinger, J. 2007.
516 Present denudation rates at selected sections of the South African escarpment and
517 the elevated continental interior based on cosmogenic ^3He and ^{21}Ne . *South African*
518 *Journal of Geology* 110(2-3), 235-248.

519 Lal, D., 1991. Cosmic ray labeling of erosion surfaces: in situ nuclide production rates
520 and erosion models. *Earth and Planetary Science Letters* 104(2-4), 424-439.

521 LeMasurier, W.E. 1987. Mount Hampton. *Volcanoes of the Antarctic Plate and southern*
522 *oceans*, 189-194.

523 LeMasurier, W.E., Kawachi, Y. 1990. Mount Hampton. In LeMasurier, W.E. and
524 Thomson, J.W. (eds) *Volcanoes of the Antarctic plate and southern oceans*.
525 American Geophysical Union, Antarctic Research Series 48, 189-194.

526 LeMasurier, W.E., Rex, D.C., 1989. Evolution of linear volcanic ranges in Marie Byrd
527 Land, west Antarctica. *Journal of Geophysical Research: Solid Earth* 94(B6), 7223-
528 7236.

529 LeMasurier, W.E., Rocchi, S., 2005. Terrestrial record of post-Eocene climate history
530 in Marie Byrd Land, West Antarctica. *Geografiska Annaler. Series A. Physical*
531 *Geography*, 51-66.

532 LeMasurier, W.E., Thomson, J.W. Eds 1990. *Volcanoes of the Antarctic plate and*
533 *southern oceans*. American Geophysical Union, Antarctic Research Series 48, 487
534 pp.

535 LeMasurier, W.E., Futa, K., Hole, M., Kawachi, Y. (2003). Polybaric evolution of
536 phonolite, trachyte, and rhyolite volcanoes in eastern Marie Byrd Land, Antarctica:
537 controls on peralkalinity and silica saturation. *International Geology Review* 45(12),
538 1055-1099.

539 Mabry, J., Burnard, P., Blard, P.H., Zimmermann, L., 2012. Mapping changes in helium
540 sensitivity and peak shape for varying parameters of a Nier-type noble gas ion
541 source. *Journal of Analytical Atomic Spectrometry* 27(6), 1012-1017.

542 Margerison, H.R., Phillips, W.M., Stuart, F.M., Sugden, D.E. (2005) An assessment of
543 cosmogenic ³He surface exposure dating in the Northern Dry Valleys of East
544 Antarctica. *Earth and Planetary Science Letters* 230, 163-175.

545 Marrero, S.M., Phillips, F.M., Borchers, B., Lifton, N., Aumer, R., Balco, G., 2016.
546 Cosmogenic nuclide systematics and the CRONUScale program. *Quaternary*
547 *Geochronology* 31, 160-187.

548 Marrero, S.M., Hein, A.S., Naylor, M., Attal, M., Shanks, R., Winter, K., Sugden, D.
549 2018. Controls on subaerial erosion rates in Antarctica. *Earth and Planetary Science*
550 *Letters* 501, 56-66.

551 Masarik, J., 2002. Numerical simulation of in situ production of cosmogenic nuclides.
552 *Geochimica Cosmochimica Acta* 66 (15A), A491.

553 Matsuda, J., Matsumoto, T., Sumino, H., Nagao, K., Yamamoto, J., Miura, Y.,
554 Kaneoka, I., Takahata, N., Sano, Y., 2002. The ³He/⁴He ratio of the new internal He
555 Standard of Japan (HESJ). *Geochemical Journal* 36(2), 191-195.

556 Matsuoka, N., Moriwaki, K., Hirakawa, K. (1996). Field experiments on physical
557 weathering and wind erosion in an Antarctic cold desert. *Earth Surface Processes*
558 *and Landforms* 21(8), 687-699.

559 Middleton, J.L., Ackert, R.P., Mukhopadhyay, S., 2012. Pothole and channel system
560 formation in the McMurdo Dry Valleys of Antarctica: new insights from
561 cosmogenic nuclides. *Earth and Planetary Science Letters* 355, 341-350.

562 Mukhopadhyay, S., Ackert, R.P., Pope, A.E., Pollard, D., DeConto, R.M., 2012.
563 Miocene to recent ice elevation variations from the interior of the West Antarctic ice
564 sheet: Constraints from geologic observations, cosmogenic nuclides and ice sheet
565 modeling. *Earth and Planetary Science Letters* 337, 243-251.

566 Nicolas, J.P., Bromwich, D.H., 2014. New reconstruction of Antarctic near-surface
567 temperatures: Multidecadal trends and reliability of global reanalyses. *Journal of*
568 *Climate* 27(21), 8070-8093.

569 Nishiizumi, K., Kohl, C.P., Arnold, J.R., Klein, J., Fink, D., Middleton, R., 1991.
570 Cosmic ray produced ^{10}Be and ^{26}Al in Antarctic rocks: exposure and erosion history.
571 Earth and Planetary Science Letters 104(2-4), 440-454.

572 Oberholzer, P., Baroni, C., Schaefer, J.M., Orombelli, G., Ochs, S.I., Kubik, P.W.,
573 Baur, H., Wieler, R., 2003. Limited Pliocene/Pleistocene glaciation in Deep Freeze
574 Range, northern Victoria Land, Antarctica, derived from in situ cosmogenic
575 nuclides. Antarctic Science 15(04), 493-502.

576 Panter, K.S., Hart, S.R., Kyle, P., Blusztajn, J., Wilch, T., 2000. Geochemistry of Late
577 Cenozoic basalts from the Crary Mountains: characterization of mantle sources in
578 Marie Byrd Land, Antarctica. Chemical Geology 165(3), 215-241.

579 Parai, R., Mukhopadhyay, S., Lassiter, J.C., 2009. New constraints on the HIMU
580 mantle from neon and helium isotopic compositions of basalts from the Cook-
581 Austral Islands. Earth and Planetary Science Letters 277(1), 253-261.

582 Paulsen, T.S., Wilson, T.J. 2010. Evolution of Neogene volcanism and stress patterns
583 in the glaciated West Antarctic Rift, Marie Byrd Land, Antarctica. Journal of the
584 Geological Society 167(2), 401-416.

585 Peizhen, Z., Molnar, P., and Downs, W. R. 2001. Increased sedimentation rates and
586 grain sizes 2–4 My ago due to the influence of climate change on erosion rates.
587 Nature 410(6831), 891.

588 Placzek, C.J., Matmon, A., Granger, D.E., Quade, J., Niedermann, S. 2010. Evidence
589 for active landscape evolution in the hyperarid Atacama from multiple terrestrial
590 cosmogenic nuclides. Earth and Planetary Science Letters 295 (1–2), 12–20.

591 Pollard, D., DeConto, R. M., 2009. Modelling West Antarctic ice sheet growth and
592 collapse through the past five million years. Nature 458(7236), 329.

593 Raymo, M.E., Lisiecki, L.E., Nisancioglu, K.H. 2006. Plio-Pleistocene ice volume,
594 Antarctic climate, and the global $\delta 18\text{O}$ record. Science 313(5786), 492-495.

595 Rocchi, S., LeMasurier, W.E., Di Vincenzo, G., 2006. Oligocene to Holocene erosion
596 and glacial history in Marie Byrd Land, West Antarctica, inferred from exhumation
597 of the Dorrel Rock intrusive complex and from volcano morphologies. Geological
598 Society of America Bulletin 118(7-8), 991-1005.

599 Ryan, J.G., Kyle, P.R., 2004. Lithium abundance and lithium isotope variations in
600 mantle sources: insights from intraplate volcanic rocks from Ross Island and Marie
601 Byrd Land (Antarctica) and other oceanic islands. Chemical Geology 212(1), 125-
602 142.

603 Seidl, M.A., 1993. Form and process in channel incision of bedrock. PhD dissertation,
604 University of California, Berkeley.

605 Seidl, M.A., Finkel, R.C., Caffee, M.W., Hudson, G.B., Dietrich, W.E., 1997. Cosmic
606 Isotope Analyses Applied to River Longitudinal Profile Evolution: Problems and
607 Interpretations. Earth Surface Processes and Landforms 22(3), 195-209.

608 Seitz, H.M., Brey, G.P., Lahaye, Y., Durali, S., Weyer, S., 2004. Lithium isotopic
609 signatures of peridotite xenoliths and isotopic fractionation at high temperature
610 between olivine and pyroxenes. Chemical Geology 212(1-2), 163-177.

611 Steig, E.J., Fastook, J.L., Zweck, C., Goodwin, I.D., Licht, K.J., White, J.W., Ackert,
612 R.P., 2001. West Antarctic ice sheet elevation changes. The West Antarctic Ice
613 Sheet: Behavior and Environment 75-90.

614 Stone, J.O., 2000. Air pressure and cosmogenic isotope production. Journal of
615 Geophysical Research: Solid Earth 105(B10), 23,753-23,759.

616 Stone, J.O., Balco, G.A., Sugden, D.E., Caffee, M.W., Sass, L.C., Cowdery, S.G.,
617 Siddoway, C., 2003. Holocene deglaciation of Marie Byrd land, west Antarctica.
618 Science 299(5603), 99-102.

- 619 Stuart, F.M., Burnard, P.G., Taylor, R., & Turner, G., 1995. Resolving mantle and
620 crustal contributions to ancient hydrothermal fluids: He-Ar isotopes in fluid
621 inclusions from Dae Hwa W-Mo mineralisation, South Korea. *Geochimica et*
622 *Cosmochimica Acta* 59(22), 4663-4673.
- 623 Stuart, F.M., Lass-Evans, S., Fitton, J.G., Ellam, R.M., 2003. High $^3\text{He}/^4\text{He}$ ratios in
624 picritic basalts from Baffin Island and the role of a mixed reservoir in mantle plumes.
625 *Nature* 424(6944), 57-59.
- 626 Sugden, D.E., Balco, G., Cowdery, S.G., Stone, J.O., Sass, L.C., 2005. Selective glacial
627 erosion and weathering zones in the coastal mountains of Marie Byrd Land,
628 Antarctica. *Geomorphology* 67(3), 317-334.
- 629 Sugden, D.E., Hein, A.S., Woodward, J., Marrero, S.M., Rodés, A., Dunning, S.M.,
630 Stuart, F.M., Freeman, S., Winter, K., Westoby, M.J., 2017. The million-year
631 evolution of the glacial trimline in the southernmost Ellsworth Mountains,
632 Antarctica. *Earth and Planetary Science Letters* 469, 42-52.
- 633 Tabushi, M., 1958. Solvent Extraction of Beryllium as Acetylacetonate. *Bulletin of the*
634 *Institute for Chemical Research, Kyoto University* 36(6), 156-162.
- 635 Van der Wateren, F.M., Dunai, T.J., Van Balen, R.T., Klas, W., Verbers, A.L.,
636 Passchier, S. and Herpers, U., 1999. Contrasting Neogene denudation histories of
637 different structural regions in the Transantarctic Mountains rift flank constrained by
638 cosmogenic isotope measurements. *Global and Planetary Change* 23(1), 145-172.
- 639 Williams, A.J., Stuart, F.M., Day, S.J., Phillips, W.M., 2005. Timing and rate of
640 landscape development in central Gran Canaria, eastern Atlantic Ocean, from
641 cosmogenic ^3He concentrations in pyroxene microphenocrysts. *Quaternary Science*
642 *Reviews* 24, 211-222.
- 643 Wysoczanski, R.J., Gamble, J.A., Kyle, P.R., Thirlwall, M.F., 1995. The petrology of
644 lower crustal xenoliths from the Executive Committee Range, Marie Byrd Land
645 volcanic province, West Antarctica. *Lithos* 36(3-4), 185-201.
- 646 Xu, S., Dougans, A.B., Freeman, S.P., Schnabel, C., Wilcken, K.M., 2010. Improved
647 ^{10}Be and ^{26}Al -AMS with a 5 MV spectrometer. *Nuclear Instruments and Methods in*
648 *Physics Research Section B: Beam Interactions with Materials and Atoms* 268(7-8),
649 736-738.